17 April 1998

ELSEVIER

Chemical Physics Letters 286 (1998) 490–496

CHEMICAL PHYSICS LETTERS

Microscopic determination of the interlayer binding energy in graphite

Lorin X. Benedict [a,1], Nasreen G. Chopra [a], Marvin L. Cohen [a], A. Zettl [a], Steven G. Louie [a], Vincent H. Crespi [b]

[a] *Department of Physics, University of California at Berkeley and Materials Sciences Division, Lawrence Berkeley National Laboratory, Berkeley, CA 94720, USA*

[b] *Department of Physics, 104 Davey Laboratory, Pennsylvania State University, University Park, PA 16802-6300, USA*

Received 15 July 1997; in final form 21 October 1997

Abstract

High-tensile-strength carbon nanotubes are nonetheless susceptible to large radial deformations. In particular, tubes may collapse so that opposing tube walls attain the graphitic interlayer spacing. A simple elastic model shows that the ratio of mean curvature modulus to the interwall attraction of graphite determines the cross-section of a collapsed tube. Transmission electron microscopy of collapsed tubes confirms the elastic model and affords the first microscopic measurement of the strength of the intersheet attraction, a quantity otherwise difficult to assess. © 1998 Elsevier Science B.V.

1. Introduction

Literature values for the energy of attraction between graphite layers differ by a factor of a hundred. Empirical interatomic interactions fit to a database of hydrocarbon binding energies, a two-parameter interatomic potential fit to the c-axis compressibility and the interlayer spacing of graphite, and application of intermolecular N_2 interaction potentials to carbon atoms all yield weak interlayer attractions of $\varepsilon_{attr} \approx 0.002$, 0.002, and 0.003 eV/atom respectively [1–3]. In contrast, local density approximation (LDA) calculations yield $\varepsilon_{attr} \approx 0.02$ eV/atom [4–6] and $\varepsilon_{attr} \approx 0.03$ eV/atom (M. Côté, private communication). Bear in mind that the LDA can have difficulty with the correlation-born Van der Waals energy. Alternative theoretical calculations and semiempirical estimates yield a clutch of larger values, $\varepsilon_{attr} \approx 0.04$, 0.1, 0.17, 0.2 eV/atom [7–10]. A single heat of wetting experiment yields $\varepsilon_{attr} \approx 0.04$ eV/atom [11]. Although this value is in reasonable agreement with the difference between a bond-energy sum and the graphite heat of vaporization [12], this estimate is the difference of large, imprecisely known numbers.

Our measurement exploits the well-known mean curvature modulus of graphite in a unique experimental geometry which balances curvature energy with the interlayer attraction [13,14]. A carbon nan-

[1] Present address: Optical Technology Div., Physics Laboratory, National Institute of Standards and Technology, Gaithersburg, MD 20878, USA.

PII S0009-2614(97)01466-8

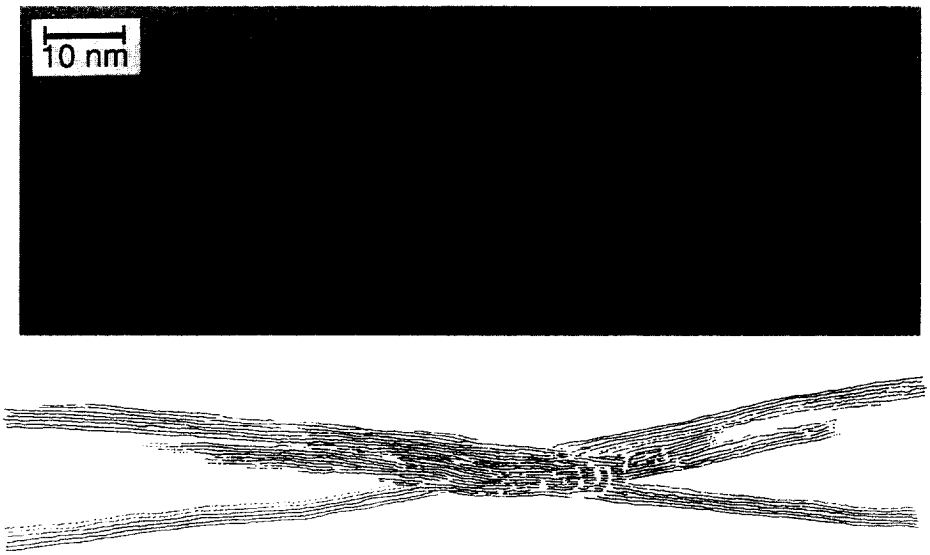

Fig. 1. A flattened twisted nanotube. Extra bulb-derived walls appear on the upper portion of the nanotube. Lateral Moire smudges are visible near the crossover region. The line drawing emphasizes the main features of the twist.

otube [15] can collapse into a flat strip with bulbs on the edges [16], the large radial deformations being stabilized by the intersheet attraction [2] between opposing sides of the inner wall. Collapse is favored in large tubes: as tube circumference increases, the excess curvature energy in the bulbs asymptotes to a constant while the energetic advantage of the intersheet attraction increases linearly. The ratio of the interlayer attraction to the graphitic mean curvature modulus determines the size of the bulbs and the radius above which collapse is favored. Careful analysis of transmission electron microscopy (TEM) images of flattened, twisted tubes reveals the size of the bulbs, allowing us to extract the strength of the interlayer binding, $0.035^{+0.015}_{-0.01}$ eV/atom, while simultaneously exploring the detailed morphology.

2. Experiment

Carbon nanotube samples were synthesized by the standard arc method [17]. Nanotubes were transferred to holey carbon grids by rubbing the material between glass slides. The samples were then imaged in a JEM JEOL 200CX TEM operating at 200 keV. Of three examples of twisted flattened nanotubes that proved suitable for further analysis, we will concentrate on Fig. 1. Previous sample rotation [16] confirms that the tube is uniformly collapsed along its length. The flattening persists in untwisted regions, showing that the collapse is stabilized by intersheet attraction and is not maintained by an external torque [18].

We first analyze the apparent width as shown in Fig. 2. The fit for constant twist angle of $\alpha = 0.02 \pm 0.002$ rad/nm is satisfactory with a hint of a slight asymmetry. We observe two Moire periods in the central region: a poorly defined Moire period of 2.7 ± 0.4 nm in the center of the crossover and a better-defined halved period of 1.4 ± 0.2 nm at the edges of the crossover. The smaller spacing at the edges of the crossover implies a crossing angle of 0.24 ± 0.03 radians between sets of planes 3.35 Å apart, an angle which implies $\alpha = 0.24 \pm 0.03$ rad $\div$ 14 ± 1 nm $= 0.017 \pm 0.002$ rad/nm, consistent with the twist rate derived from the apparent width. The brief and poorly defined period doubling in the center of the crossover suggests a halving of the crossing angle, consistent with Moire patterns arising from two sets of planes from the bulbs interacting with the atomic planes from the central portion of

[2] We refrain from calling this term the Van der Waals energy because other correlation-borne and kinetic contributions to the interlayer binding energy may also be important.

the tube, planes which produce maximal contrast at the center of the crossover.

Closer study of the tube walls reveals roughly eight additional contrast lines rising from the mist on the inner side of the upper eight original walls on either side of the twist. These extra walls arise from the bulbs on the edges of the flattened tube. Their appearance at roughly 40 nm from the crossover indicates that atomic planes in the bulbs tilt at an angle of roughly 35 ± 5 degrees from edge-on. [3]

The appearance of the extra walls on just the upper side means that the bulbs do not bulge symmetrically on either side of the flat region, but instead bulge to just one side, as shown in Fig. 3. This unusual structure reflects a symmetry-breaking cupping deformation of a twisted ribbon. Consider first the elastic deformations of a twisted sheet as opposed to a twisted flattened tube. A twisted sheet with a straight cross-section has a nonzero Gaussian curvature. [4] Such a shape is strongly disfavored by the large Gaussian curvature modulus of graphite. A cupped cross-section can remove this Gaussian curvature. Describing the cross-section of the twisted sheet by $f(x)$ (with the screw axis passing through $x = 0$), the condition of zero Gaussian curvature yields a nonlinear differential equation,

$$f''(xf' - f) = \left(1 + (f')^2\right)^2. \qquad (1)$$

Since the right-hand side is always positive, the curvature f'' has constant sign, consistent with a cupped geometry. The constraint that $f''(xf' - f) \geqslant 0$ guarantees that the solution does not curve away from the origin when $f' = 0$. In a tube (as opposed to a sheet) the cupping concentrates in the already-bent bulbs, flattening one side and accentuating the other with a lesser curvature introduced into the previously flat region between the bulbs. The concentration of cupping in the bulbs is evidenced by the restricted region of enhanced alignment in the center of the twist in Fig. 1, which can only be

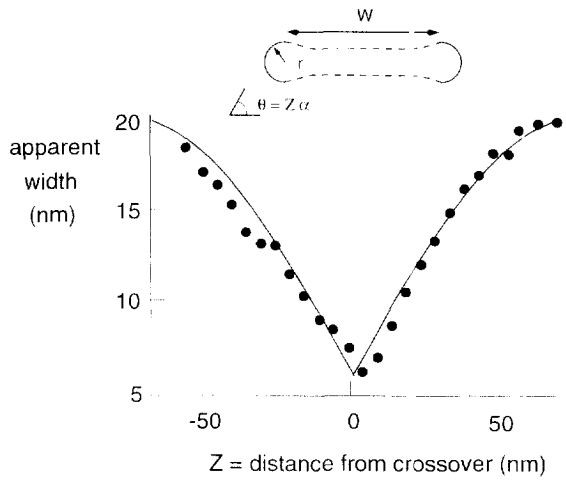

Fig. 2. Experimental results and fit to the form $W \sin \alpha Z + 2r = 14 \sin 0.02Z + 6$ nm for the apparent width of the twisted nanotube of Fig. 1.

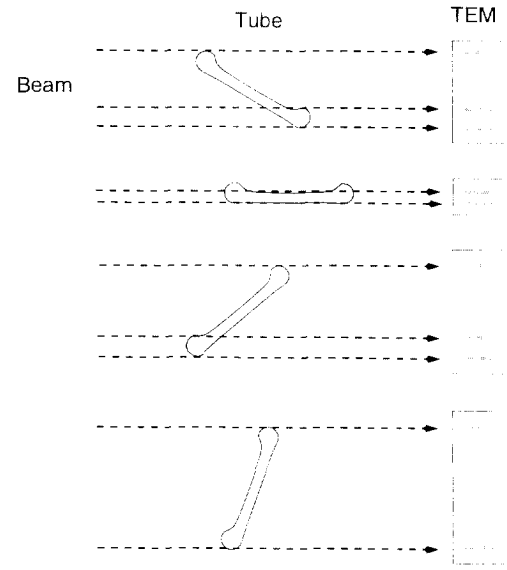

Fig. 3. The left-hand side depicts the rows of atoms which give the maximum contrast in projected potential as the tube is rotated. A schematic of the TEM image appears on the right-hand side. Extra lattice planes due to the bulbs appear on only one side of the nanotube image. For clarity only a single wall is shown and the central portion is drawn as perfectly flat.

[3] The large angle at which the bulbs are seen is attributed to the cupping instability (to be described later), which concentrates the bulb on one side of the tube.

[4] The Gaussian curvature is $(\lambda/2\pi)^2/((\lambda/2\pi)^2 + x^2)^2$ where λ is the length of the twist along the screw axis, and x points perpendicular to the screw axis, which is located at $x = 0$.

explained if the central region is nearly flat. Fig. 3 [5] shows how the cupping instability accounts for the appearance of extra walls on just one side of the image.

The minimum spacing between the bulb-derived walls and the primary walls is not the graphitic interwall spacing but instead the diameter of the bulb. Fig. 1 shows this spacing on the left of the crossover. The gap slowly shrinks from 10 ± 1 Å to 7 ± 1 Å before closing abruptly. The minimum spacing, 7 ± 1 Å, is a good approximation to the diameter of the inner bulb. [6] Extraction of the interlayer binding energy from this information requires an elastic theory which describes the size and shape of the bulbs.

3. Elastic model

Opposing walls of a flattened multiwall nanotube collapse to an optimum distance d apart. If the graphite sheets do not tear, then the two flat sections must join at the edges. If $\varepsilon_{\text{attr}} d^2 \sim k$, the graphite sheet mean curvature modulus [19], then the edges bulge smoothly to decrease the local curvature energy, yielding the cross-section shown in Fig. 4. We model the bulbs as semicircles joined smoothly to the flat region by identical curves $\alpha \sin(\beta x + \gamma) + \delta$. The interwall distance is fixed at d in the flat and semicircular sections, but is slightly less than d in the sine portions. The deviation from d in the sine portion will be small as long as r is not too much larger than $d/2$, an assumption consistent with the actual bulb dimensions. In this arrangement the difference in perimeters between successive layers is $2\pi d$ in both circular and collapsed configurations.

Four parameters then determine the shape of the N-walled collapsed tube: the interlayer distance d, the radius r of the inner semicircle in the bulb, the length L of the flat region and the outer perimeter $2\pi R$ of the collapsed tube, written as the circumference of the corresponding circular tube. As long as R is much larger than a typical graphite intersheet spacing, the distance d between flat walls is always nearly 3.35 Å (the graphitic value). Thus, we fix $d = 3.35$ Å for all tubes. We then minimize the sum of the curvature and intersheet attraction energies as a function of (r, L) for different tube perimeters $2\pi R$. All energies are defined per unit axial length.

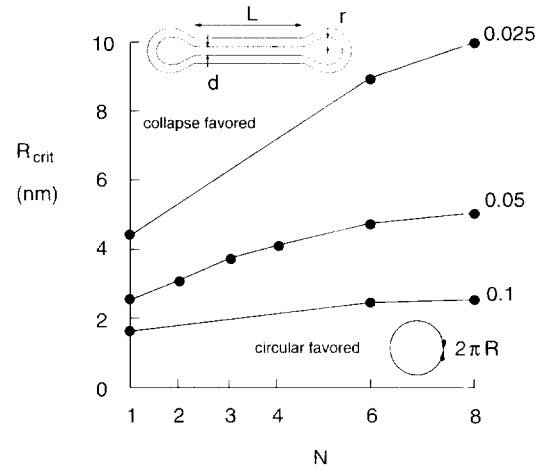

Fig. 4. Critical radius for tube stability R_{crit}, as a function of the number of walls N, calculated with $\varepsilon_{\text{attr}} = 0.1$, 0.05, 0.025 eV/atom. For small N and large R collapsed tubes are favored. The parameterizations for the cross-sections of the flattened and circular tubes are also shown.

The curvature energy of a circular tube with radius $R \gg d$ is

$$\frac{k}{2}\frac{(2\pi R)}{R^2} = \frac{\pi k}{R}.$$

This expression accurately fits ab initio calculations of the total energies of circular carbon tubes [20] when $k = 1.4$ eV. As long as R is large, k is independent of the helicity of the tube because the in-plane elastic properties of a graphite sheet are isotropic. The bulbs in a collapsed nanotube define a surface with one-dimensional translational symmetry which has a curvature energy of

$$\frac{k}{2}\int \frac{\mathrm{d}l}{[R(x)]^2} = \frac{k}{2}\int \mathrm{d}x \frac{[f''(x)]^2}{\{1 + [f'(x)]^2\}^{5/2}} \qquad (2)$$

for a cross-section defined by $y = f(x)$.

[5] The external forces which stabilize a twist sometimes also enforce a bend. For a tube simultaneously twisted and bent no solution exists with zero Gaussian curvature everywhere. TEM images of such situations (unpublished) reveal kinks which concentrate the Gaussian curvature in a small region of severely disrupted material.

[6] The influence of the cupping distortion on the size of the bulb is negligible compared to the errors in the direct measurement of the bulb size.

The energy of intersheet attraction is calculated by partitioning the cylindrical surface into axial strips of infinitesimal width w and summing the Lennard–Jones interaction over pairs of strips. The Lennard–Jones interaction between two parallel, infinitely long strips is

$$V_{LJ}(D) = -\frac{s}{D^5} + \frac{t}{D^{11}}, \qquad (3)$$

where D is the distance between strips and $s,t > 0$. The coefficients s and t are determined by two constraints: the interaction energy between infinite sheets is a minimum at $D = d$ and the binding energy per area at this distance is $-\varepsilon_{attr}$. We obtain $s = 1.2505 w^2 \varepsilon_{attr} d^4$ and $t = 0.8204 w^2 \varepsilon_{attr} d^{10}$.

Eq. (3) contains an inconvenient divergence from neighboring points in the same layer. Formally, the divergence is inconsequential since it is eliminated by referencing all energies to the (equally divergent) graphite sheet Lennard–Jones energy. Practically, we eliminate divergent terms by excluding contributions between portions of a single surface whose inward normals make an angle less than a certain cutoff angle. The final result for the interlayer attraction is insensitive to the cutoff angle over a wide range, with $\theta = 130°$ being suitable for all tubes studied.

The relevant parameter for the elastic theory is ε_{attr}/k, which determines the size of the bulbs and the crossover between circular and collapsed configurations. Bulbs are larger for smaller ε_{attr}/k since the loss of attraction between opposite sides of the inner wall is proportional to $\varepsilon_{attr} r$ while the curvature energy goes like k/r. Thus, $r \sim (\varepsilon_{attr}/k)^{1/2}$.

Bulb diameters have been extracted for three collapsed tubes, yielding the results shown in Table 1. Our direct measurements of bulb size rule out both the lower and upper sets of estimates for the intersheet attraction ($\varepsilon_{attr} = 0.002$–$0.003$ eV/atom and 0.1–0.2 eV/atom). Instead, they support the heat of wetting experiments and/or the LDA results. In retrospect, the groupings of values around 0.002 and 0.2 eV/atom were suspect since they are sensitive to the choice of empirical force law and/or did not address the unique strongly anisotropic bonding geometry of graphite.

Table 1
Experimental collapsed tube parameters, along with the ε_{attr} that would yield these results in our model. N is the number of walls and R is the inner radius of the corresponding cicular tube

N	R (nm)	Bulb diameter (Å)	ε_{attr} (eV/atom)
8	5.2	7 ± 1	0.05 ± 0.02
6	7.4	8 ± 2	$0.04 \pm 0.04 - 0.02$
8	5.2	9 ± 1.5	$0.02 \pm 0.02 - 0.01$
Average			$0.035^{+0.015}_{-0.01}$

The energy of interaction between graphitic layers depends somewhat on the type of stacking. Although multiwalled nanotubes cannot maintain perfect interlayer registration, the wrapping indices of adjacent layers within a nanotube are often very similar (D. Bernearts, personal communication). We expect the interlayer registration in our samples to be intermediate between turbostratic and perfect (e.g. Bernal) graphite. Note that the slightly larger interlayer spacing in circular nanotubes relative to Bernal graphite is not firm evidence for poor interlayer registration, since the nanotube interlayer distance is fixed at the high temperature of formation and decreases only slightly under cooling [21].

The elastic theory also yields the critical radius R_{crit} at which a collapsed tube with inner circumference $2\pi R_{crit}$ is degenerate with the corresponding circular tube. Because the attractive energy lowering after collapse is roughly independent of the number of walls N, and the curvature energy gain increases with N, $R_{crit}(N)$ is an increasing function of N. Fig. 4 shows a plot of $R_{crit}(N)$ for $1 \leqslant N \leqslant 8$.[7] For $\varepsilon_{attr} = 0.05$ eV/atom the inner-wall bulb radius r decreases from 4.7 Å to 3.6 Å as the number of walls increases from 1 to 8. Since the energetic barrier towards collapse is much larger than $k_B T$, tube geometries are most likely dominated by kinetics. How large must R be for the collapsed form to be metastable? A collapsed tube with a straight section has an attractive interaction between opposing walls which maintains its structure. Without it, the tube will return to a circular cross-section to release the curvature energy. This suggests that $R_{meta}(N) \approx R_{crit}(N) - \pi^{-1} L_{crit}(N)$, where $L_{crit}(N)$ is the length

[7] In Ref. [16], we estimated R_{crit} for a few different N, and obtained values that are larger than those reported here. We have since refined the model, and take the present predictions to be the most accurate.

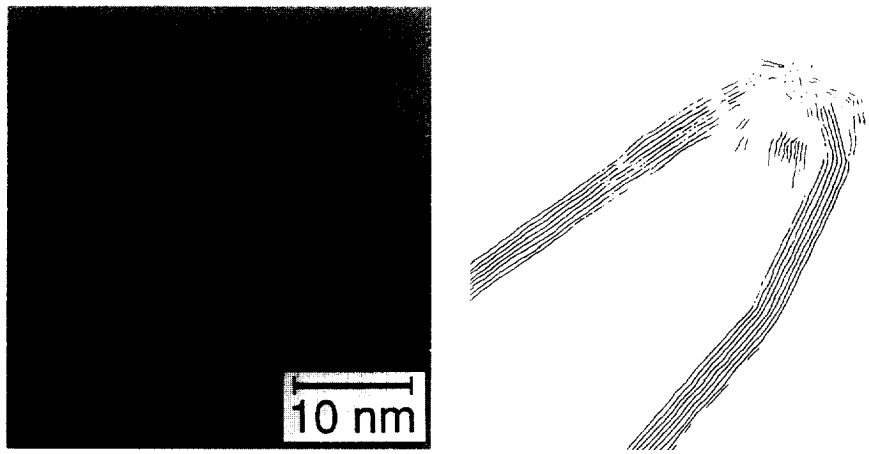

Fig. 5. The end of a collapsed tube. Contrast lines are severely disrupted at the apex. Additional contrast lines appear inward from the cap region, unlike the undistorted cappings observed for circular tubes.

of the straight portion of the inner wall for a collapsed tube with $R = R_{crit}$. Again, $R_{meta}(N)$ increases with N: $R_{meta}(1) \approx 13.6$ Å and $R_{meta}(8) \approx 14.6$ Å (for $\varepsilon_{attr} = 0.05$ eV/atom), a relatively weak dependence on N.

Do tubes grow while flattened, or flatten after synthesis? The rigid cap at the end of the nanotube precludes post-synthesis flattening all the way to the end of the tube. Fig. 5 shows the cap of a flattened nanotube. The appearance of extra contrast lines interior of the edge of the cap is not seen in the cappings of circular tubes [22]. These extra contrast lines can be explained as the bulging of the flattened portion as it approaches the rigid perpendicular structure of the cap. Since it is unlikely that such a highly strained distorted cap structure would form in situ during synthesis, this cap distortion suggests that the tube was circular during growth. In fact, a rough estimate suggests that the mechanical advantage of rubbing a sparse sample of nanotubes between glass slides is sufficient to flatten a fraction of the nanotubes. The tubes were most likely flattened during post-synthesis handling.

4. Summary

Continuum elasticity theory with a Lennard–Jones description of intersheet attraction yields the equilibrium cross-sections of collapsed carbon nanotubes. Tubes with few walls and large radii favor collapse over the more familiar circular cross-section. The size of the bulbs on the edges of collapsed tubes depends on the ratio of the intersheet attraction to the mean curvature modulus. Detailed analysis of TEM images of twisted collapsed tubes allows us to extract the number of walls, tube radii, and bulb sizes, while analysis of Moire patterns and apparent widths determines the twist angle. Comparison of theory and experiment affords a measurement of the graphite intersheet attractive energy, $0.035^{+0.015}_{-0.01}$ eV/atom. The ends and kinks of these tubes are consistent with the properties expected for nanotubes which collapse after formation.

Acknowledgements

This research was supported by the National Science Foundation Grant No. DMR-9520554 and by the Office of Energy Research, Office of Basic Energy Sciences, Materials Sciences Division of the U.S. Department of Energy under Contract No. DE-AC03-76SF00098. NGC acknowledges support from the Department of Education. AZ and SGL acknowledge support from the Miller Institute for Basic Research in Science.

References

[1] N.L. Allinger, J. Am. Chem. Soc. 99 (1977) 8127
[2] J.T. Sprague, N.L. Allinger, J. Comput. Chem. 1 (1980) 257.
[3] A.A. Ahmadieh, H.A. Rafizadeh, Phys. Rev. B 7 (1973) 4527.

[4] J.-C. Charlier, X. Gonze, J.-P. Michenaud, Europhys. Lett. 28 (1994) 403.
[5] M.C. Schabel, J.L. Martins, Phys. Rev. B 46 (1992) 7185.
[6] J.-C. Charlier, J.-P. Michenaud, Phys. Rev. Lett. 70 (1993) 1858.
[7] A.D. Crowell, J. Chem. Phys. 22 (1954) 1397.
[8] E. Santos, A. Villagrá, Phys. Rev. B 6 (1972) 3134.
[9] R.O. Brennan, J. Chem. Phys. 20 (1952) 40.
[10] R. Setton, Carbon 33 (1995) 1135.
[11] L.A. Girifalco, R.A. Lad, J. Chem. Phys. 25 (1956) 693, and references therein.
[12] H.J. Bernstein, Trans. Faraday Soc. 58 (1962) 2285.
[13] R.S. Ruoff, J. Tersoff, D.C. Lorents, S. Subramoney, B. Chan, Nature 364 (1993) 514.
[14] J. Tersoff, R.S. Ruoff, Phys. Rev. Lett. 73 (1994) 676.
[15] S. Iijima, Nature 354 (1991) 56.
[16] N.G. Chopra, L.X. Benedict, V.H. Crespi, M.L. Cohen, S.G. Louie, A. Zettl, Nature 377 (1995) 13518.
[17] W. Kratschmer, L.D. Lamb, K. Fostiropoulos, D.R. Huffman, Nature 364 (1993) 514.
[18] B.I. Yakobson, C.J. Brabec, J. Bernholc, Phys. Rev. Lett. 76 (1996) 2511.
[19] S.A. Safran, Statistical Thermodynamics of Surfaces and Interfaces, Addison-Wesley, Reading, MA 1994.
[20] X. Blase, A. Rubio, S.G. Louie, M.L. Cohen, Europhys. Lett. 28 (1994) 335.
[21] S. Amelinckx, D. Bernhaerts, X.B. Zhang, G. Van Tendeloo, J. Van Landuyt, Science 267 (1995) 1334.
[22] S. Iijima, Mater. Sci. Eng. B 19 (1993) 172.